

Continual Online Personalization of Exoskeleton Control via Manifold-Aware Experience Replay

Changseob Song and Inseung Kang, *Member, IEEE*

Abstract—Personalizing exoskeleton control remains a critical challenge for clinical users with gait disabilities. Online adaptation (OA) offers an effective solution by adapting in real time to subject variability, device fit, and diverse locomotor tasks. However, OA involves a continual stream of user state data, which can lead to catastrophic forgetting of previously learned locomotor contexts. Here, we develop a manifold-aware experience replay-based online personalization framework designed to maintain user-specific representations across diverse tasks during OA of exoskeleton control. By replaying previously experienced tasks from a replay buffer, we preserve the personalized exoskeleton assistance across all learned tasks. Furthermore, we capture a gait manifold that distinguishes between different locomotor tasks, removing the need for explicit task labeling when selecting target replay bins. We evaluated our framework on emulated hemiplegic gait, which largely deviates from able-bodied patterns, across multiple forgetting scenarios with speed and incline transitions. Our manifold-aware replay framework achieved 40% and 60% improvements in torque and gait phase tracking accuracy, respectively, compared to a baseline framework without replay, which exhibited catastrophic forgetting during task transitions. This demonstrates that our proposed framework personalizes exoskeleton control in real time across diverse locomotor contexts in daily ambulation of clinical populations.

Index Terms—Exoskeleton personalization, online adaptation, continual learning, manifold-aware experience replay, multi-modal locomotion.

I. INTRODUCTION

Robotic exoskeletons are increasingly intervening into our daily lives, offering a meaningful contribution to community ambulation [1]–[3]. Beyond improving the walking economy of able-bodied users [1], exoskeletons have demonstrated benefits for clinical populations with motor impairments by improving walking economy [4]–[7], gait stability [7]–[10], pain [11], [12], and user preference [13], [14]. While several studies have developed exoskeleton controllers that successfully improve gait outcomes for clinical users, these controllers rely on manual tuning of control parameters [4], [6], [8] and extensive optimization time for each target subject [7]. Personalizing exoskeleton control rapidly, within a short amount of user experience, and efficiently, without a labor-intensive tuning process, has therefore become an important agenda in the wearable robotics field. This challenge intensifies for clinical populations, such as post-stroke, where substantial inter-

subject gait variability makes effective assistance particularly difficult to achieve [15]–[17].

Recent advances in wearable robotics domain have been largely driven by machine learning (ML)-based control methods [5], [18]–[24]. Trained on large datasets spanning diverse locomotor tasks, ML-driven exoskeleton controllers have shown promise for assisting users across various real-world scenarios [19], [20], [22], [23], and can estimate diverse user states in real time, such as biological joint moment [20], [21], gait phase [5], [22]–[24], and activity mode [22], [25]–[27], which can be intuitively mapped into exoskeleton torque commands. By construction, however, these data-driven controllers are bounded by the coverage of their training distribution and degrade under out-of-distribution conditions for unseen users and tasks, requiring retraining on downstream clinical users [5], [26], [27]. This hinders the exoskeleton applicability, particularly when users cannot easily access gait labs with expensive instrumentation.

To personalize these static controllers, several studies have proposed online adaptation (OA) strategies that adjust the controller toward target users and tasks in real time [5], [26]–[28]. OA has shown promise in accommodating user gait variability, differences in device fit relative to the pre-trained hardware setup, and sensor signal shift induced by torque application. For instance, Kang *et al.* developed an OA framework that adapts a gait phase estimator toward stroke gait in real time [5], and Johnson *et al.* online-adapted walking speed estimators for prosthetic applications [28]. While these studies successfully personalized user state estimators in real time, their implementation was restricted to single-task scenarios. Exoskeleton personalization, however, requires the controller to adapt concurrently across a wide range of locomotor tasks, which single-task frameworks cannot provide.

In continual learning scenarios involving multiple tasks, models are susceptible to catastrophic forgetting, in which information from previously learned tasks is lost through overfitting to the current task [29]–[31]. To mitigate this, the ML community has developed diverse solutions, including experience replay, regularization, and architecture-based methods [29]–[31]. Among these, experience replay is one of the most effective approaches, storing previously encountered experiences and replaying them throughout continual adaptation to maintain stability across the diverse locomotor tasks a user encounters during OA [32]. In the wearable robotics field, experience replay has so far been applied to prosthetic studies, including a pipeline that replays bins across different walking speeds [26] and a stability-plasticity balancing pipeline that adjusts the learning rate and the replayed task [27]. While successful within the prosthetics domain,

This work was supported in part by the NIH R21 Award 1R21EB037268-01 and in part by the Kwanjeong Educational Foundation. Corresponding author: Changseob Song, changseob@cmu.edu.

This work involved human subjects or animals in its research. Approval of all ethical and experimental procedures and protocols was granted by the Carnegie Mellon University Institutional Review Board.

C. Song and I. Kang are with the Department of Mechanical Engineering, Carnegie Mellon University, Pittsburgh, PA 15213, USA.

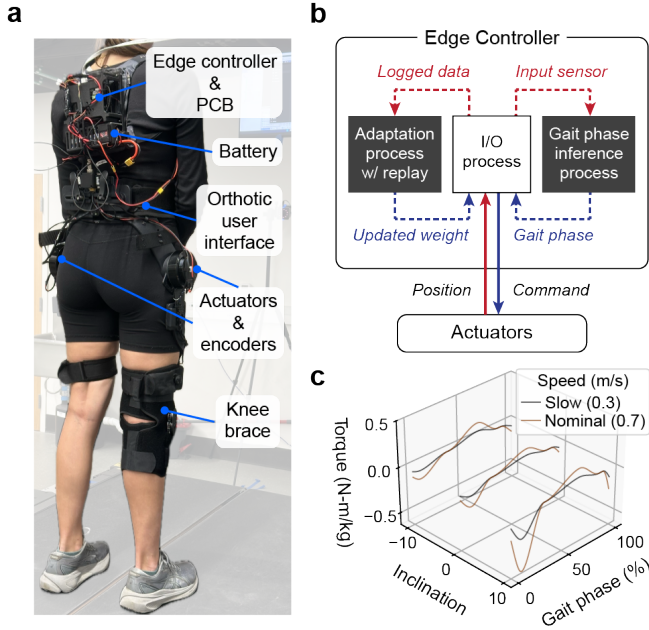


Fig. 1. Hip exoskeleton hardware and software. (a) Robotic hip exoskeleton designed to assist the user’s bilateral hip motion during locomotion. (b) Real-time control flow within the edge controller unit. Dashed lines indicate inter-process communication between parallel software modules, while solid lines show peripheral communication between the controller’s I/O process and the physical actuators. Black shaded boxes show GPU-accelerated processes, and the white box indicates a CPU-centric process. (c) Spline profiles for different walking inclines and speeds. This mid-level spline profile maps high-level gait phase into low-level torque command.

these approaches leave two limitations unaddressed. First, no exoskeleton study has demonstrated OA across multimodal task contexts, particularly under the sparser sensing modalities available to exoskeletons relative to prosthetic devices. Second, prior studies [26], [27] assume that task labels are known when organizing the replay bins, an assumption that does not hold in real-world deployment.

In this work, we incorporate gait manifold-aware experience replay into the OA of exoskeleton control for users with hemiplegic gait patterns, addressing the two limitations above. We online-adapt a hip exoskeleton gait phase estimator, whose output is mapped into a torque profile to deliver effective assistance; because gait phase is a universal high-level user state, adapting the estimator ensures the assistance timing that maximizes exoskeleton performance [5], [33], [34]. To maintain stable assistance across diverse tasks, the framework continually replays previously seen locomotor tasks the user has encountered. To remove the need for explicit task labeling, it organizes the replay buffer using the encoded features of gait data, allowing target replay bins to be selected without locomotor context labels. Throughout this manifold-aware OA framework, we anticipate that the exoskeleton can deliver personalized assistance across diverse locomotor tasks while remaining stable under the continual learning conditions of real-world ambulation.

II. METHOD

A. Robotic Hip Exoskeleton

We developed a robotic hip exoskeleton capable of applying bilateral torque (Fig. 1a). The device had a total mass of 4.5 kg and provided joint torque up to 22 N·m in the sagittal plane, powered by a Lithium-Polymer battery (HRB-POWER). Two quasi-direct-drive brushless DC motors (AK80-9, CubeMars) actuated the hip joints, each equipped with an encoder that measured the hip joint kinematics. The edge controller (Jetson Orin Nano, NVIDIA) ran a CPU-centric I/O process that managed joint kinematics acquisition and torque command transmission via CAN communication at 100 Hz (Fig. 1b). Operating in parallel, a GPU-accelerated gait phase inference process estimated the user’s gait state by retrieving encoder signals through asynchronous inter-process communication. To ensure deterministic control at 100 Hz, the I/O process utilized a zero-order hold strategy, reusing the previous phase estimate when a GPU update was not available within the control cycle. Simultaneously, an adaptation process sampled gait data every three heel strikes to update the weights of the final linear layer, which were then queued back to the I/O process. These three modules operated concurrently within a parallelized software architecture.

The estimated gait phase, representing the high-level user state, was mapped to torque commands. Task context from the predefined experimental protocol selected the corresponding mid-level control splines (Fig. 1c). We obtained predefined splines for level-ground (LG) and ramp-ascent (RA) tasks from a prior study on minimizing energy expenditure [35]. Ramp-descent (RD) splines were extrapolated by scaling the LG splines according to the relationship between LG and RD biological joint moments across eleven able-bodied participants, and reference profiles were linearly scaled across speeds. The resulting torque commands were sent to the low-level controller, which used a torque-tracking loop embedded in the motor driver of the actuator assembly.

B. Gait Phase Estimation

We developed a deep learning-based gait phase estimator based on previous studies [23], [24], which served as the baseline able-bodied model and the initial seed for online personalization. The estimator was a temporal convolutional network (TCN), a widely used architecture in the exoskeleton field for modeling time-series data [20], [21]. To build the baseline model, we collected 15 hours of able-bodied data from 11 participants. The dataset spanned five inclinations of -10, -5, 0, 5, and 10 degrees. The LG data included seven speeds, from 0.2 to 1.4 m/s in 0.2 m/s increments, along with transient speed conditions, while the RD and RA conditions each included four speeds, from 0.4 to 1.0 m/s in 0.2 m/s increments, with transient conditions.

The TCN estimated the user’s gait phase from bilateral hip encoder signals, forming two input channels (Fig. 2c). We estimated the gait phase for a unilateral side to simplify the backward labeling of OA and the organization of the replay buffer. Similar to prior gait phase studies [5], [23], [24], we used a Cartesian representation ($x = \cos(\phi)$, $y = \sin(\phi)$),

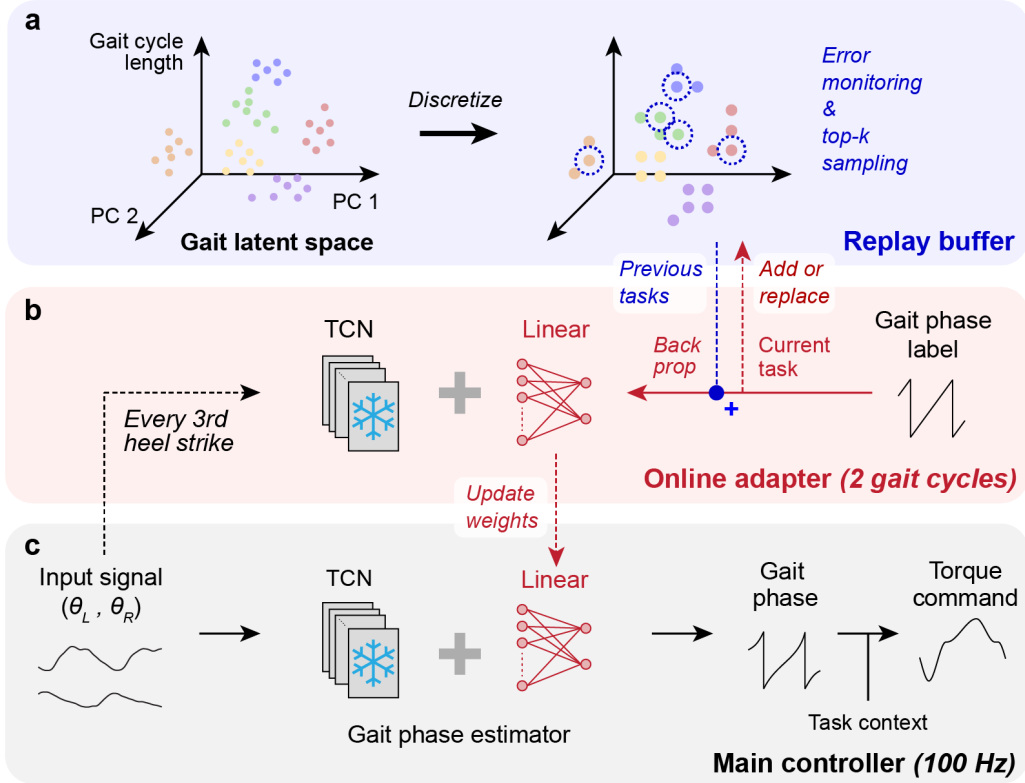


Fig. 2. Manifold-aware experience replay framework for online adaptation (OA). The overall architecture includes (a) a replay buffer within gait latent space, (b) an OA module that updates the gait phase estimator’s neural network, and (c) a main control loop that receives input signals, predicts the gait phase, and commands torque. In the main controller, the estimated gait phase is mapped into torque commands using the task context and predefined mid-level control splines in Fig. 1c. The OA module is triggered by the main controller every third heel strike and retrieves data from two gait cycles. It then generates a gait phase label that is time-synchronized with the streamed input sensor data. Using this user-specific data, the module updates the weights of the final linear layer of the temporal convolutional network (TCN), while the preceding TCN feature-extracting blocks remain frozen. The newly personalized weights are subsequently transferred to the main process. To prevent catastrophic forgetting, the adaptation module utilizes a replay buffer that saves the user’s gait manifold. As new data arrives, the buffer is updated by adding new data or replacing overlapping manifolds. The adaptation module monitors estimation accuracy across all experienced tasks, prioritizing the top four lowest-accuracy tasks to combine with the current task to form a training dataset.

where ϕ denotes the gait phase, to account for the inherent discontinuity of the gait phase profile at heel strike, where it transitions from 100% to 0%, to improve estimator performance. The model configuration, optimized via hyperparameter sweeping and leave-one-subject-out validation, used a 1-second temporal window, a two-layer dilated convolutional architecture with a kernel size of 5 and 80 channels per layer, a batch size of 16, and a learning rate of 10^{-6} . After training, the TCN blocks were exported in TensorRT format [36] to accelerate inference on the edge controller’s GPU, while the parameters of the final linear layer were exported in PyTorch format [37] to allow for real-time weight updates during the adaptation process.

C. Online Adaptation Framework

We developed an OA framework that (1) continually streamed the input data logged from the main control loop, (2) backward-labeled the gait phase, and (3) updated the estimator network weights by backpropagating with new data from the current user’s state (Fig. 2b). The main control loop triggered the OA process every third heel strike. Heel strikes were detected from ground reaction force signals streamed by a force-plate-instrumented treadmill (FIT5, Bertec) used during

the experiment. The sensor input signals were streamed to the OA process along with the heel strike indices and used to backward-label a time-synchronized gait phase. After the dataset was loaded, the final linear layer of the TCN was updated using the Adam optimizer with a learning rate of 5×10^{-5} , 50 times larger than the learning rate used to train the gait phase estimator offline. The right and left side of the estimator were updated separately to simplify the labeling and data binning processes.

We froze the high-level feature extractor, consisting of five TCN blocks, to preserve the features representing generic human locomotion, and fine-tuned only the final linear layer that maps the latent space to the gait phase. This strategy is commonly used in transfer learning to preserve general features while adapting downstream task-specific features [38]. Beyond maintaining the stability of the transfer, it also conserves computing resources and reduces update latency, particularly because the TCN blocks contain 18 times more parameters than the final linear layer in our setup.

D. Gait Manifold

We encoded a gait manifold to distinguish between multimodal locomotor tasks across varying inclines and speeds.

Algorithm 1: Online Adaptation with Manifold-Aware Experience Replay

Input: Models $\pi_{\{L,R\}}$, Params $\theta_{\{L,R\}}$, PCA Matrix Φ , Thresholds τ_{lo} , Grid intervals δ_{pc} , δ_t , Max replay number K

Output: Updated parameters θ

```

1 Initialize: Buffer  $\mathcal{B} \leftarrow \{\emptyset\}$ ,  $n_{adapt} \leftarrow 0$ 
2 while True do
3   SignalReady()           // Await next task
4    $x, side \leftarrow receive()$  // Get input & L/R side
5    $\pi, \theta \leftarrow SelectModel(side)$  // Load active
    model weights
6    $z_t \leftarrow dim_t(x)$  // Temporal length
7    $z_{pc} \leftarrow PCA(x, \Phi)$  // PC projection
8    $\kappa \leftarrow (\lfloor z_{pc}/\delta_{pc} \rfloor, \lfloor z_t/\delta_t \rfloor)$  // Compute grid key
9   if  $n_{adapt} > n_{min}$  then
    // Start binning after a minimal number
    of adaptation
10    if  $\kappa \notin \mathcal{B}[side]$  then
11       $\mathcal{B}[side][\kappa] \leftarrow x$  // Initialize new bin
12    end
13    else
14       $\mathcal{B}[side][\kappa] \leftarrow Update(x, \mathcal{B}[side][\kappa])$ 
    // Update existing bin
15    end
16  end
17   $\mathcal{E} \leftarrow \{RMSE(\pi, b) \mid b \in \mathcal{B}[side]\}$  // Evaluate
    error on all bins
18   $\mathcal{S}_{sort} \leftarrow argsort(\mathcal{E})$  // Rank bins by RMSE
19   $\mathcal{D}_{replay} \leftarrow Top_K(\{b \in \mathcal{S}_{sort} \mid \tau_{lo} < RMSE(b)\})$ 
    // Get buffer with desired RMSE range &
    select top-k
20   $\mathcal{D}_{train} \leftarrow \{x\} \cup \mathcal{D}_{replay}$  // Combine current
    and replay data
21   $\theta \leftarrow SGD(\pi, \mathcal{D}_{train})$  // Update weights
22   $n_{adapt} \leftarrow n_{adapt} + 1$ 
23  send( $\theta$ ) // Sync with main control loop
24 end

```

To maintain effective assistance across the task set, the exoskeleton control must remain task-aware, particularly when binning incoming data and replaying previous samples during OA. While the exoskeleton literature has used discrete task classifiers [22], [25], such classifiers themselves degrade under out-of-distribution conditions when encountering new, impaired gait patterns. We therefore built a feature extractor that projects gait data into a latent representation, enabling silhouette separation between tasks and preventing redundant replay of similar gait representations.

To build the feature extractor, we used the same dataset as the baseline gait phase estimator, consisting of 16,623 gait cycles. Kinematic data were segmented using reference-side heel strikes and downsampled to 50 samples per cycle, and the bilateral signals were concatenated into a 100-dimensional input vector. We applied principal component analysis to this data and retained the first two principal components, which

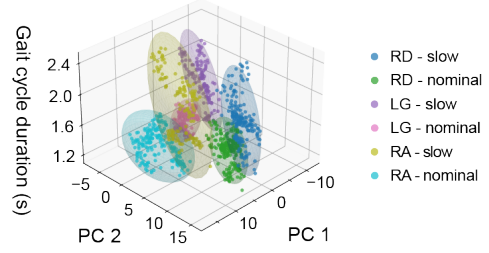


Fig. 3. Gait manifold. High-dimensional gait data were projected into a 3D latent space comprising the first two principal components, which was derived from able-bodied kinematics data, and the corresponding gait cycle duration. Each color indicates a distinct locomotor task, and ellipsoids represent the 99% confidence interval for each cluster.

accounted for 77% of the total explained variance. We then used the gait cycle duration of the reference limb as a third axis, establishing a three-dimensional latent space for gait representation (Fig. 3). The projected manifolds showed clear separation between locomotor tasks, providing a basis for manifold-aware replay without explicit task labeling. Validated on the able-bodied dataset used to develop the principal component extractor, the manifold clusters yielded a silhouette score of 0.15 across task clusters.

E. Manifold-Aware Task Replay

We developed a manifold-aware task replay technique to prevent catastrophic forgetting of previous tasks during OA (Algorithm 1). Using the gait latent space (Fig. 3), we designed a binning process that allocated new bins for unseen manifolds and replaced past samples with recent data for redundant manifolds. When OA was triggered by new gait data, the data was projected into the latent space through the principal component transformation. To avoid maintaining an unbounded number of replay bins, we discretized the projected manifold using a predefined grid-key interval. The binning process was initiated only after a minimum of four adaptations for each new user, ensuring stabilization. If the discretized location was novel, a new bin was added; otherwise, the existing bin was replaced with the new data. After binning, we assessed the current model’s performance by tracking the root mean square error (RMSE) of all existing bins against the ground truth, and retained only bins with RMSE values between 2.5% and 20% to ensure efficient and stable replay. We then selected the top four bins, a value optimized by balancing estimation RMSE and update latency (Fig. 5b). Finally, the replay dataset was combined with the current data for backpropagation, and the updated weights were transferred to the main control loop for the gait phase estimator.

F. Hemiplegic Gait Emulation

We focused on stroke survivors as the target population because of their high inter- and intra-subject gait variability and gait asymmetry [5], [16], [17]. Beyond its clinical implications, this kinematic variability and asymmetry exacerbate distribution shifts for ML-driven exoskeleton controllers, which is particularly critical for controllers relying on sparse

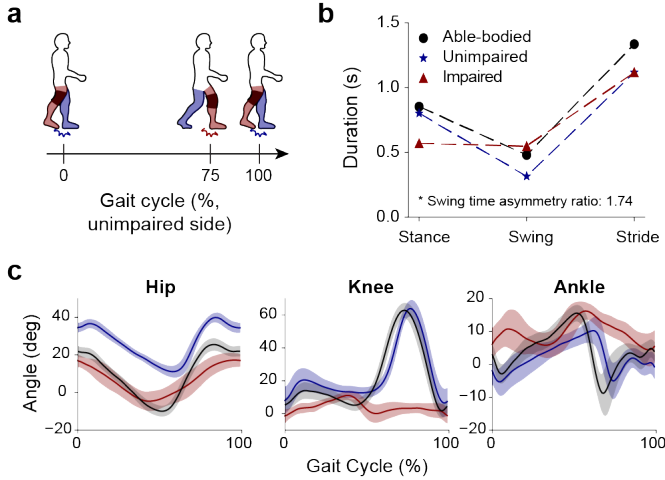


Fig. 4. Emulated hemiplegic gait. (a) Gait cycle timing of impaired- and unimpaired-side heel strikes. (b) Stance, swing, and stride durations of emulated gait. (c) Sagittal plane joint kinematics of the emulated gait (mean \pm SD, $n = 3$) compared to able-bodied gait.

sensor observations such as the bilateral hip encoders used in this study. To reproduce these conditions in able-bodied participants, we fitted a knee brace on the right knee to emulate stiff-knee gait (Fig. 1a), and provided metronome cues that instructed participants to time their heel strikes to induce gait asymmetry (Fig. 4a). The audio cues were set to align the impaired-side heel strike with the 75% mark of the non-impaired side’s gait cycle. Stride durations were set to 1.1 and 1.4 seconds for slow and nominal speeds used in the experimental protocol (Fig. 6a). Preliminary results from three subjects confirmed that the emulated hemiplegic gait at the nominal speed deviated substantially from the able-bodied data, averaged across the 11 subjects used to train the baseline estimator, in both stance and swing durations. The resulting swing time asymmetry ratio was 1.74 (Fig. 4b), closely matching the temporal characteristics of stroke survivors reported in previous studies [16], [17]. Lower-limb kinematics at the hip, knee, and ankle joints also showed clear deviations and asymmetry compared to able-bodied patterns. To ensure that subjects adapted properly to the emulated gait, they completed an adaptation period of at least five minutes across various speeds before the main experiment.

G. Experimental Protocol

We recruited nine able-bodied subjects (7 male, 2 female) with a body mass of 68.3 ± 12.3 kg and a height of 173.1 ± 4.7 cm. The experimental protocol included six locomotor tasks with varying speeds and inclines (Fig. 6a). Subjects first performed all six unseen tasks for 30 seconds each, ensuring that the exoskeleton control personalized to every task for the target user (Tasks 1–6). The controller was then exposed to a single task for five minutes to induce a forgetting scenario, such as LG slow or LG nominal (Task 7). Finally, the controller was tested on the remaining five tasks for 10 seconds each (Task 8), yielding five forgetting-testing pairs. Although the task conditions were run as separate trials, the network weights and replay buffers were transferred from each

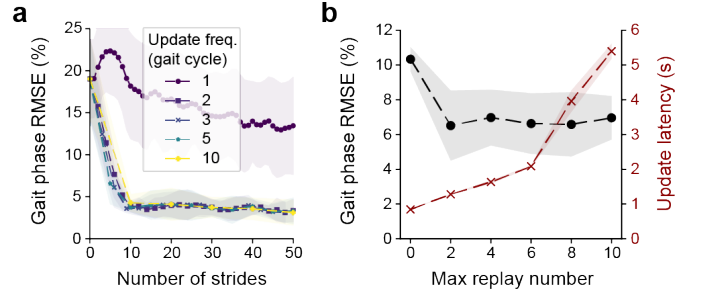


Fig. 5. Effect of update parameters in offline data streaming simulation. (a) Effect of update frequency on gait phase error (mean \pm SD, $n = 4$). (b) Effect of maximum replay number on gait phase error and update latency (mean \pm SD, $n = 2$).

trial to the next. Every trial began with 10 seconds of gait stabilization before the subject reached steady-state walking and adaptation began. Each subject completed the same protocol for both the baseline framework, which adapted without replay, and the proposed manifold-aware replay framework, with the framework order randomized across subjects.

H. Statistical Analysis

A two-way analysis of variance (ANOVA) was performed to evaluate the effects of adaptation method, adapted without replay versus manifold-aware replay, and locomotor condition on torque tracking error. To identify specific differences between methods within each condition, *post-hoc* pairwise comparisons were conducted using paired t-tests, and all p -values were adjusted using the Bonferroni correction.

III. RESULTS

A. Effect of Update Parameters on Online Adaptation

For a fixed number of strides, we analyzed the effect of update frequency on estimator performance in an offline environment that mirrored the online control frequency and streamed pre-recorded emulated hemiplegic gait data. Update frequencies greater than one gait cycle yielded similar accuracy, whereas updating every gait cycle slowed convergence considerably (Fig. 5a). This was primarily due to the 1-second TCN window, which limited the usable training data to the duration remaining after one second was subtracted from each gait cycle. Consequently, although a one-cycle update is the most frequent, it produced the greatest convergence delay. We therefore chose an update frequency of two gait cycles to ensure rapid convergence, triggering OA every third heel strike so that the system retained sufficient processing time by skipping one gait cycle after each pair.

We also optimized the maximum number of replays. Because data loading and backpropagation time scale with the replay number, we selected a value that yielded update accuracy comparable to higher replay numbers while maintaining sufficiently low update latency, defined as the interval between the update trigger and the arrival of new network parameters at the main loop. We evaluated estimator performance and update latency using the same protocol (Fig. 6a), with data pre-recorded during pilot experiments. A maximum of four

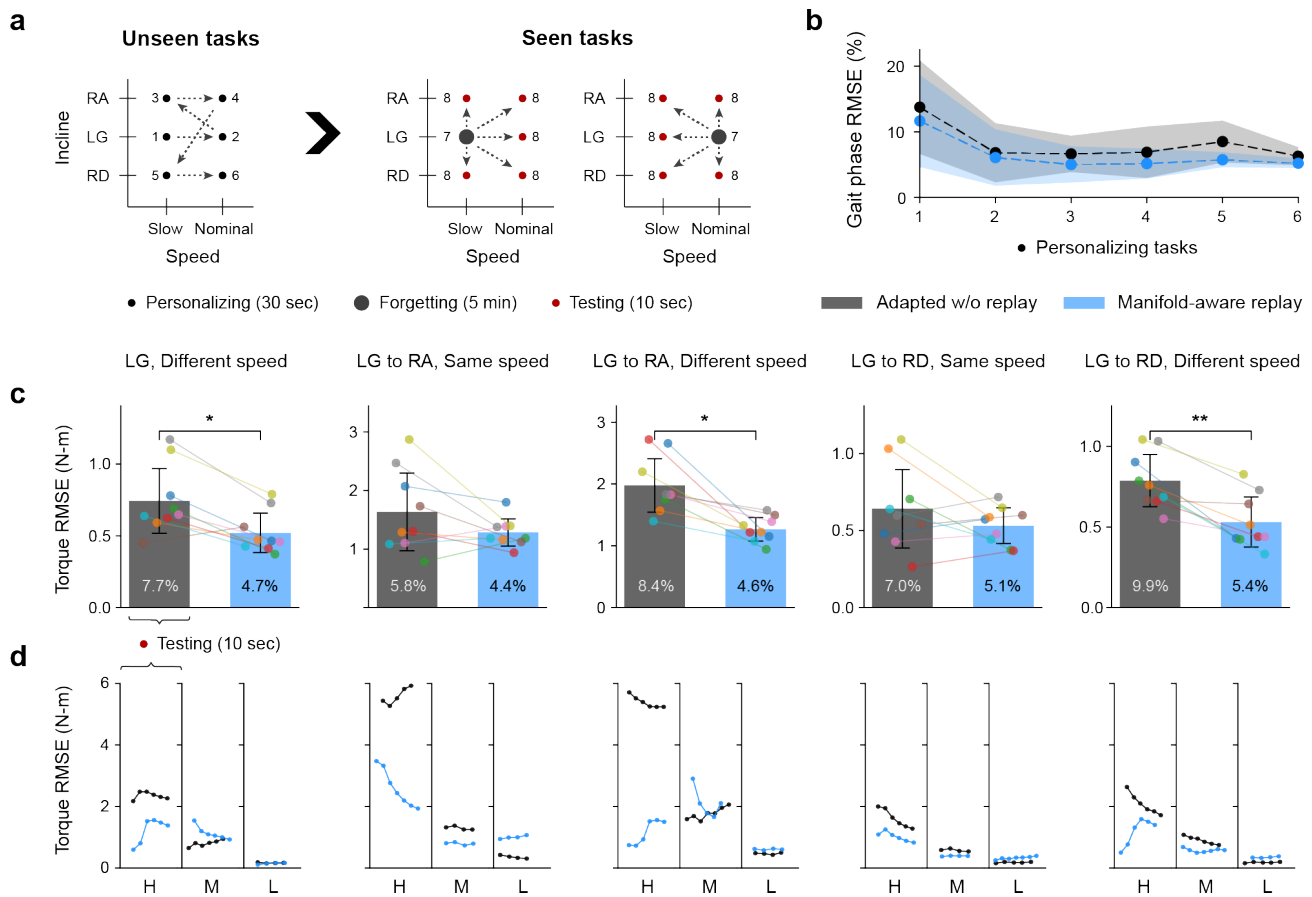


Fig. 6. Experimental protocol and the results. (a) Experimental protocol across six locomotor tasks with the 1) personalization (Tasks 1–6), 2) forgetting (Task 7), and 3) testing (Task 8) phases. (b) Gait phase RMSE during the personalization phase across novel locomotor tasks (mean \pm SD, $n = 9$). (c) Torque RMSE across five forgetting-testing pairs during the testing phase. Colored markers represent individual subjects. Asterisks denote statistical significance (* $p < 0.05$, ** $p < 0.01$). Inscripted numeric values on the bar graphs indicate the corresponding mean gait phase RMSE for each condition. (d) Representative forgetting scenarios for the five forgetting-testing pairs. Subplots categorize the highest (H), median (M), and lowest (L) torque error cases across all subjects, tasks and limbs. Each marker corresponds to a single gait cycle during the 10-second testing window.

replay bins kept the update latency under two seconds while maintaining accuracy comparable to higher numbers, so we adopted that value (Fig. 5b).

B. Main Experiment

Using the protocol described in Fig. 6a, the main experiment showed that both the baseline and proposed methods began with a high gait phase error around 15% during the first task of the personalization phase (Fig. 6b). After the initial personalizing task, errors for both cases stabilized under 10%. Throughout the personalization phase, the manifold-aware method resulted in 1.7% less error across all novel tasks compared to the baseline.

To analyze performance during the testing phase, we evaluated five different forgetting-testing task pairs: 1) LG, different speed, 2) LG to RA, same speed, 3) LG to RA, different speed, 4) LG to RD, same speed, and 5) LG to RD, different speed. Each pair comprised two testing trials from both LG slow and LG nominal forgetting cases. To assess tracking performance, torque RMSE was calculated between the online torque commands and the ground-truth torque labels generated retrospectively from the task context and gait phase labels. The

bar graph in Fig. 6c shows values averaged across the testing duration, both limbs, and two testing trials for each of the five task pairs.

Overall, the manifold-aware replay method reduced torque RMSE by 40% compared to the baseline. For the five specific task pairs, error reductions were 43%, 27%, 56%, 21%, and 48%, respectively. Significant improvements were observed in the (LG, different speed) and (LG to RA, different speed) pairs ($p < 0.05$), with the most significance found in the (LG to RD, different speed) pair ($p < 0.01$). Furthermore, the proposed method exhibited a higher torque RMSE than the baseline in only 1, 3, 0, 5, and 0 subjects across the five task pairs. Even in the task pairs with 1, 3, and 5 subjects, the differences, 0.11, 0.26, and 0.09 N-m, respectively, were negligible relative to the overall error scale. For gait phase RMSE, the proposed method achieved a 60% improvement compared to the baseline. Fig. 6d illustrates representative forgetting scenarios categorized by the highest (H), median (M), and lowest (L) baseline torque RMSE, among all subjects, testing tasks, and limb sides. For the highest-error cases, the baseline error consistently exceeded that of the proposed method.

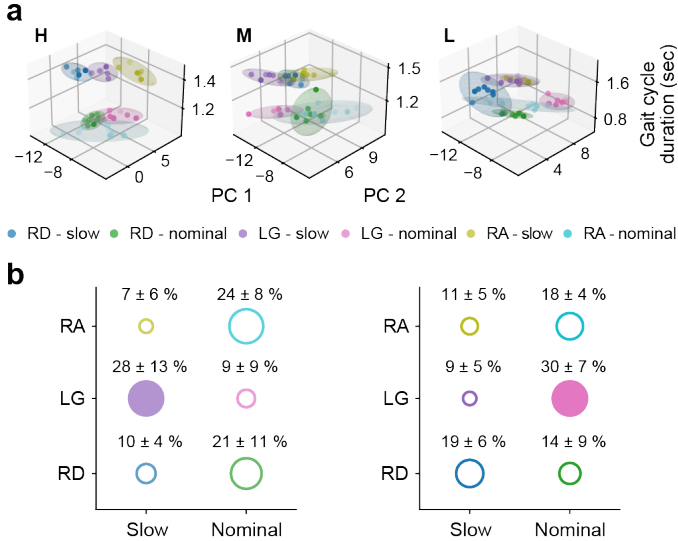


Fig. 7. (a) Gait manifolds shown for individuals with the highest, median, and lowest silhouette scores, projected using the principal component extractor derived in Fig. 3. Each color indicates a distinct locomotor task, and ellipsoids represent the 90% confidence intervals. (b) Replay distributions during the forgetting phase for LG slow and LG nominal tasks. Filled markers denote the ongoing tasks during the forgetting phase.

C. Replay Distribution and Latency

Post-hoc manifold clustering reveals that the six locomotor tasks performed during the personalization phase formed largely distinct representations within the gait latent space. Figure 7a illustrates the cases with the highest, median, and lowest silhouette scores among the nine testing subjects, yielding silhouette scores of 0.22, 0.07, and -0.05, respectively. The mean silhouette score across all testing subjects was 0.08 ± 0.09 . Fig. 7b shows the task replay distribution during each of the two 5-minute forgetting trials. This data was analyzed retrospectively by referencing the task labels recorded with each replay bin, but these labels were not used to select the target replay bins during the online experiment. The results show that the ongoing tasks (i.e., LG slow and LG nominal) were replayed most frequently. Meanwhile, the RA and RD tasks with different speeds from the ongoing task were the second most frequently replayed.

Fig. 8 illustrates the logged update latency recorded during the experiments. After the exoskeleton had encountered approximately four tasks, the update latency plateaued at roughly 1.5 seconds, which corresponds to the maximum replay number of four. Throughout the plateau period, the update latency remained within a band of 1.5 ± 0.3 seconds, with peak latency never exceeding three seconds.

IV. DISCUSSION

In this work, we proposed a manifold-aware replay-based OA framework for rapid adaptation to the hemiplegic gait patterns of target users. Compared to the baseline without experience replay, the proposed framework reduced torque tracking error and gait phase error by 40% and 60%, respectively. The baseline was susceptible to catastrophic forgetting of previously experienced tasks due to overfitting on the current

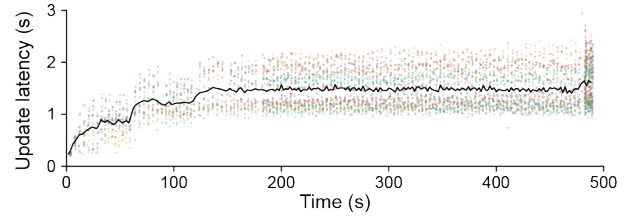


Fig. 8. Update latency throughout the experiment. The black line represents the average update latency across all subjects, and each dot indicates the latency per individual update, with colors showing different subjects.

task, whereas our manifold-aware replay technique replayed previously seen tasks without requiring locomotor context labels, an advantage for real-world deployments where such labels are difficult to obtain. The average update latency was 1.5 seconds, enabling prompt network updates that respond immediately to user needs.

The torque and gait phase RMSE results show that the baseline without manifold-aware experience replay suffers from forgetting across diverse task transitions. This forgetting was strongest in test pairs involving different speeds, more so than incline transitions alone, likely due to larger kinematic differences between speeds than between inclines. Even for task pairs involving incline transitions at the same speed, however, approximately one-third of subjects exhibited significant forgetting in the baseline.

Freezing the TCN blocks proved effective for preserving high-level, general gait features during OA. This is confirmed in Fig. 6b, where tasks following the initial task maintained lower gait phase errors, indicating that user-specific features in the final linear layer were effectively updated. Isolating the roles of individual layers in representing generic versus subject-specific gait remains difficult, as these representations are often deeply coupled, and the final linear layer is prone to overfitting on continuously streamed data, particularly during prolonged exposure to a single task. Integrating manifold-aware experience replay with this architectural strategy is therefore essential for maintaining controller stability across a diverse task set.

The replay distribution in Fig. 7 shows that tasks were heterogeneously replayed during the forgetting phase. Although ongoing task data was integrated and replayed alongside the target replay tasks, the ongoing tasks were replayed most frequently, likely reflecting a balancing mechanism that manages representation conflicts between task sets. Tasks involving different speeds and inclines were the second most frequently replayed, consistent with their largest performance improvement over the baseline in both torque and gait phase tracking.

Although this study introduces a novel manifold-aware experience replay for exoskeleton control, several limitations remain. First, retrospective gait phase labeling relied on force plate data. In real-world applications, this labeling should be offloaded to portable sensing modalities such as pressure-sensing insoles or inertial measurement units.

Furthermore, this framework adapts a gait phase estimator, which primarily updates the high-level user state, while relying

on mid-level control profiles derived from prior able-bodied studies [35]. For holistic personalization, these profiles should also be personalized, particularly for clinical populations with high inter-subject variability. This could be addressed by adopting other user state estimators such as biological torque estimators [20], [21], which depend less on fixed mid-level parameters; retrospective labeling of user states, however, remains a persistent challenge for supervised adaptation. A promising alternative is reinforcement learning (RL)-based adaptation [39], [40], which could tune mid-level control or learn end-to-end strategies, though rapid RL adaptation across diverse, unstructured tasks remains an open challenge in the exoskeleton field.

This study used a fixed learning rate, which may not suit diverse gait transition scenarios that demand a balance between rapid adaptation to new tasks and long-term stability for previously experienced tasks. Future work will explore scheduling mechanisms for both learning rates and replay counts by tracking training loss or other stability-plasticity metrics from the continual learning domain [27], and will implement logic to suspend adaptation when further updates are unnecessary.

Finally, the target users in this study walked with an emulated hemiplegic gait, which may not fully capture the complexities of real-world stroke survivors. Future work will recruit patients to investigate biomechanical challenges such as increased intra-subject gait variability and its impact on OA performance.

V. CONCLUSION

We developed a manifold-aware experience replay-based OA framework capable of personalizing exoskeleton control for hemiplegic gait across diverse locomotor tasks. By leveraging a gait manifold to replay previously experienced tasks without the need for manual task labeling, our proposed method reduced torque tracking and gait phase estimator errors by 40% and 60%, respectively, compared to a baseline method without experience replay. This framework enables online personalization to remain stable across the diverse locomotor contexts encountered during the daily ambulation of potential clinical users.

ACKNOWLEDGMENTS

The authors would like to thank Weijie Lim, Cole Drake, Atri Dey, and David Newsom who helped with the data collection, everyone who participated as subjects in the experiments, all the students in the hip exoskeleton team, Maria Tagliaferri, Jimin An, Rajiv Joshi, and Yunliang Zhao, who were involved in developing the hardware.

REFERENCES

- [1] G. S. Sawicki, O. N. Beck, I. Kang, and A. J. Young, "The exoskeleton expansion: improving walking and running economy," *Journal of neuroengineering and rehabilitation*, vol. 17, no. 1, p. 25, 2020.
- [2] S. Gao *et al.*, "Wearable technologies for assisted mobility in the real world," *Nature Communications*, vol. 16, no. 1, Dec. 2025.
- [3] C. Siviý *et al.*, "Opportunities and challenges in the development of exoskeletons for locomotor assistance," *Nature biomedical engineering*, vol. 7, no. 4, pp. 456–472, 2023.
- [4] K. Pruyn, R. Murray, L. Gabert, K. B. Foreman, and T. Lenzi, "Portable hip exoskeleton improves walking economy for stroke survivors," *Nature Communications*, vol. 17, no. 1, Feb. 2026.
- [5] I. Kang, D. D. Molinaro, D. Park, D. Lee, P. Kunapuli, K. R. Herrin, and A. J. Young, "Online adaptation framework enables personalization of exoskeleton assistance during locomotion in patients affected by stroke," *IEEE Transactions on Robotics*, vol. 41, p. 4941–4959, 2025.
- [6] A. J. Gunnell *et al.*, "Powered knee exoskeleton improves sit-to-stand transitions in stroke patients using electromyographic control," *Communications Engineering*, vol. 4, no. 1, 2025.
- [7] L. N. Awad *et al.*, "A soft robotic exosuit improves walking in patients after stroke," *Science Translational Medicine*, vol. 9, no. 400, Jul. 2017.
- [8] D. Archangeli *et al.*, "Exoskeleton frontal and sagittal plane hip torque improves propulsion and transient stability during walking in individuals with hemiparesis," *Journal of NeuroEngineering and Rehabilitation*, May 2026.
- [9] Z. F. Lerner, D. L. Damiano, and T. C. Bulea, "A lower-extremity exoskeleton improves knee extension in children with crouch gait from cerebral palsy," *Science Translational Medicine*, vol. 9, no. 404, p. eaam9145, 2017.
- [10] J. Kim *et al.*, "Soft robotic apparel to avert freezing of gait in parkinson's disease," *Nature Medicine*, vol. 30, no. 1, p. 177–185, Jan. 2024.
- [11] N. V. Divekar, E. H. Hinojosa, J. Zhang, and R. D. Gregg, "A task-agnostic knee exoskeleton for reducing osteoarthritis pain across activities of daily life: A pilot study," in *2025 International Conference On Rehabilitation Robotics (ICORR)*. IEEE, May 2025, p. 1437–1443.
- [12] J. Zhang, N. V. Divekar, E. H. Hinojosa, and R. D. Gregg, "A task-agnostic hip exoskeleton for osteoarthritis pain relief: Energetic control across activities of daily life," in *2025 International Conference On Rehabilitation Robotics (ICORR)*. IEEE, May 2025, p. 1299–1306.
- [13] K. A. Ingraham, C. D. Remy, and E. J. Rouse, "The role of user preference in the customized control of robotic exoskeletons," *Science Robotics*, vol. 7, no. 64, Mar. 2022.
- [14] U. H. Lee *et al.*, "User preference optimization for control of ankle exoskeletons using sample efficient active learning," *Science Robotics*, vol. 8, no. 83, Oct. 2023.
- [15] D. A. Winter, "Kinematic and kinetic patterns in human gait: Variability and compensating effects," *Human Movement Science*, vol. 3, no. 1–2, p. 51–76, Mar. 1984.
- [16] S. J. Olney and C. Richards, "Hemiparetic gait following stroke. part i: Characteristics," *Gait & Posture*, vol. 4, no. 2, p. 136–148, Apr. 1996.
- [17] B. Balaban and F. Tok, "Gait disturbances in patients with stroke," *PM&R*, vol. 6, no. 7, p. 635–642, Jan. 2014.
- [18] S. Luo *et al.*, "Experiment-free exoskeleton assistance via learning in simulation," *Nature*, vol. 630, no. 8016, p. 353–359, 2024.
- [19] I. Park, C. Song, and I. Kang, "Learning hip exoskeleton control policy via predictive neuromusculoskeletal simulation," 2026.
- [20] D. D. Molinaro *et al.*, "Task-agnostic exoskeleton control via biological joint moment estimation," *Nature*, vol. 635, no. 8038, pp. 337–344, 2024.
- [21] D. D. Molinaro, I. Kang, and A. J. Young, "Estimating human joint moments unifies exoskeleton control, reducing user effort," *Science Robotics*, vol. 9, no. 88, Mar. 2024.
- [22] D. Lee, S. Lee, and A. J. Young, "Ai-driven universal lower-limb exoskeleton system for community ambulation," *Science Advances*, vol. 10, no. 51, Dec. 2024.
- [23] I. Kang *et al.*, "Real-time gait phase estimation for robotic hip exoskeleton control during multimodal locomotion," *IEEE Robotics and Automation Letters*, vol. 6, no. 2, pp. 3491–3497, 2021.
- [24] I. Kang, P. Kunapuli, and A. J. Young, "Real-time neural network-based gait phase estimation using a robotic hip exoskeleton," *IEEE Transactions on Medical Robotics and Bionics*, vol. 2, no. 1, pp. 28–37, 2020.
- [25] I. Kang, D. D. Molinaro, G. Choi, J. Camargo, and A. J. Young, "Subject-independent continuous locomotion mode classification for robotic hip exoskeleton applications," *IEEE Transactions on Biomedical Engineering*, vol. 69, no. 10, p. 3234–3242, Oct. 2022.
- [26] J. Y. Maldonado-Contreras *et al.*, "Real-time adaptation of deep learning walking speed estimators enables biomimetic assistance modulation in an open-source bionic leg," *IEEE Transactions on Medical Robotics and Bionics*, vol. 7, no. 2, pp. 711–722, 2025.
- [27] C. B. Johnson, J. Maldonado-Contreras, K. R. Herrin, and A. J. Young, "Real-time balancing of stability and plasticity in continual learning enables adaptive speed estimation for lower-limb prostheses," *IEEE Transactions on Medical Robotics and Bionics*, vol. 7, no. 4, pp. 1634–1645, 2025.

- [28] C. Johnson, J. Cho, J. Maldonado-Contreras, S. Chaluvadi, and A. J. Young, "Adaptive lower-limb prosthetic control: Towards personalized intent recognition & context estimation," in *2023 International Symposium on Medical Robotics (ISMR)*, 2023, pp. 1–7.
- [29] L. Wang, X. Zhang, H. Su, and J. Zhu, "A comprehensive survey of continual learning: Theory, method and application," *IEEE Transactions on Pattern Analysis and Machine Intelligence*, vol. 46, no. 8, p. 5362–5383, Aug. 2024.
- [30] M. Delange *et al.*, "A continual learning survey: Defying forgetting in classification tasks," *IEEE Transactions on Pattern Analysis and Machine Intelligence*, p. 1–1, 2021.
- [31] M. Mermillod, A. Bugajska, and P. Bonin, "The stability-plasticity dilemma: investigating the continuum from catastrophic forgetting to age-limited learning effects," *Frontiers in Psychology*, vol. Volume 4, 2013.
- [32] D. Rolnick, A. Ahuja, J. Schwarz, T. P. Lillicrap, and G. Wayne, "Experience replay for continual learning," 2018.
- [33] A. J. Young, J. Foss, H. Gannon, and D. P. Ferris, "Influence of power delivery timing on the energetics and biomechanics of humans wearing a hip exoskeleton," *Frontiers in Bioengineering and Biotechnology*, vol. 5, Mar. 2017.
- [34] P. Slade, M. J. Kochenderfer, S. L. Delp, and S. H. Collins, "Personalizing exoskeleton assistance while walking in the real world," *Nature*, vol. 610, no. 7931, p. 277–282, Oct. 2022.
- [35] P. W. Franks *et al.*, "The effects of incline level on optimized lower-limb exoskeleton assistance: A case series," *IEEE Transactions on Neural Systems and Rehabilitation Engineering*, vol. 30, pp. 2494–2505, 2022.
- [36] NVIDIA, "NVIDIA TensorRT," 2026, accessed: April 27, 2026. [Online]. Available: <https://developer.nvidia.com/tensorrt>
- [37] A. Paszke *et al.*, "Pytorch: An imperative style, high-performance deep learning library," in *Advances in Neural Information Processing Systems* 32, 2019, pp. 8024–8035.
- [38] J. Yosinski, J. Clune, Y. Bengio, and H. Lipson, "How transferable are features in deep neural networks?" in *Advances in Neural Information Processing Systems*, vol. 27, 2014.
- [39] J. Zhong *et al.*, "Reinforcement learning control of a physical robot device for assisted human walking without a simulator," in *Proceedings of the 42nd International Conference on Machine Learning*, ser. ICML'25. JMLR.org, 2025.
- [40] Q. Zhang, Y. Chen, M. Lewek, J. Si, and H. Huang, "Towards adaptive optimal personalization control of robotic hip exoskeleton assistance for individuals with paretic stroke," *IEEE Transactions on Biomedical Engineering*, p. 1–12, 2026.